

**Title here**

Elio Campitelli \* and Leandro Díaz

*CIMA UBA blablabla*

Carolina Vera

<sup>5</sup> \**Corresponding author:* Elio Campitelli, elio.campitelli@cima.fcen.uba.ar

## ABSTRACT

Enter the text of your abstract here. This is a sample American Meteorological Society (AMS)  $\text{\LaTeX}$  template. This document provides authors with instructions on the use of the AMS  $\text{\LaTeX}$  template. Authors should refer to the file `amspaper.tex` to review the actual  $\text{\LaTeX}$  code used to create this document. The `template.tex` file should be modified by authors for their own manuscript.

10 *Significance statement.* This is significant because I wrote it.

## 11 **1. Introduction**

12 yada yada SAM yada yada circulation.. yada yada so important. yada yada many impacts.

## 13 **2. Methods**

### 14 **1) DATA**

15 We used monthly geopotential height at 2.5 longitude by 2.5 latitude resolution from ERA5  
16 (Hersbach et al.) for the period 1979 to 2018 (inclusive).

17 Monthly temperature NOAA Global Surface Temperature (NOAAGlobalTemp) 5.0 degree lati-  
18 tude x 5.0 degree longitude global grid (Vose et al. 2012; Smith et al. 2008). The same analysis  
19 was carried out using CRUTEM4 (Osborn and Jones 2014) (not shown).

20 We used monthly precipitation data from CPC Merged Analysis of Precipitation (Xie and Arkin  
21 1997) 2.5 degree latitude x 2.5 degree longitude.

### 22 **2) DEFINITION OF INDICES**

23 We defined the Southern Annular Mode (SAM) as the leading EOF of the monthly anomalies of  
24 geopotential field at 700 hPa south of 20°S (citation?). The EOF was performed by computing the  
25 Singular Value Decomposition of the data matrix consisting in 481 rows and 4176 columns (144  
26 points of longitude and 29 points of latitude). The values were weighted by the square root of the  
27 cosine of latitude to account for the non-equal area of each gridpoint (Chung and Nigam 1999).  
28 This same method was used at the rest of the levels considered in this paper.

29 To separate between the zonally symmetric and asymmetric components of the SAM, we com-  
30 puted the zonal mean and anomalies of the full SAM spatial pattern. The results are shown in

31 Figure 5 for 700hPa. The full spatial signal ( $\text{EOF}_1(\lambda, \phi)$ ) is the sum of the zonally asymmetric  
32 ( $\text{EOF}_1^*(\lambda, \phi)$ ) and symmetric ( $[\text{EOF}_1](\lambda, \phi)$ ) components. We then compute the “Full”, “Asym-  
33 metric” and “Symmetric” indices, by regressing each geopotential field on these patterns (weighting  
34 by the cosine of latitude).

35 The three indices are normalised by dividing them by the standard deviation of the “Full” index  
36 at each level. This means that comparing the magnitude between indices is meaningful, but it also  
37 means that not every index will have unit standard deviation.

### 38 3) SIGNIFICANCE

39 We adjusted p-values for False Detection Rate following Wilks (2016).

## 40 3. Results

41 Figure~6 shows the resulting Asymmetric and Symmetric time series corresponding to 700 and  
42 30hPa. blablababla

- 43 • stratosphere clearly nor normally distributed. a lot of values near 0 and some relatively high  
44 outliers. Especially true int he case of the asymmetric index. High frequency variability.
- 45 • In both levels, there’s correlation between the series (expected),

46 Correlations between the Asymmetric and Symmetric series are rather constant throught the  
47 troposphere, fluctiating between 0.39 and 0.45 (Figure~7). Futhermore, the cross-correlation of  
48 each series across levels –shown in Figure~8– are high in the trosposphere (greater than 0.9)  
49 for both indices. This suggests that both the Asymmetric and the Symemtric component of  
50 the tropospheric SAM are highly vertically coherent, both in their individual evolution and their  
51 temporal relationship. This is to be expected since the SAM is mostly equivalent barotropic  
52 (citaaaa).

53 In the stratosphere the situation is different. As can be seen in Figure~7, the relationship between  
54 the Asymmetric and Symmetric indices varies with height above 100 hPa. It starts to decrease right  
55 over the tropopause, reaches a minimum of 0.21 at 20 hPa and then it increases again monotonically  
56 with height up to the uppermost level of the reanalysis. The cross-correlation across levels in  
57 the stratosphere is generally weaker than in the troposphere (Figure~8). Furthermore, above 100  
58 hPa, the cross-correlation decreases more rapidly with height for the Symmetric SAM than for  
59 the Asymmetric SAM as evidenced by the wider dark red areas near the diagonal in Figure~8b)  
60 vs. Figure~8c). Moreover, the stratospheric Symmetric SAM seems to be slightly more connected  
61 to the troposphere than the Asymmetric SAM; this can be seen by the lower correlation values in  
62 the top right quadrant of Figure~8b) in comparison with Figure~8c).

63 Figure~8a) show the cross-correlation across levels for the Full SAM index. . . . .

64 To understand the spatial patterns associated with both indices we regressed monthly geopotential  
65 anomalies into both indices using multiple regression (Figure A6 illustrates the difference between  
66 computing two simple regressions and one multiple regression).

67 Figure~9 shows the spatial year-long regression for selected levels. In the troposphere the Full  
68 annular mode is clearly “contaminated” with well known zonal asymmetries (panels g and j) which  
69 are successfully separated by our methodology (panels h, i, k and l). In the stratosphere, the spatial  
70 pattern associated with the Full SAM is much more clearly dominated by a zonally symmetric,  
71 monopolar structure (panels a and d) that is, however, not perfectly centered in the south pole. The  
72 monopoles obtained by multiple regression with the Asymmetric and Symmetric SAM (panels c  
73 and f in Figure~9) is much more symmetric and the shift from total symmetry is captured by the  
74 regression pattern of the Asymmetric SAM as a wave-1 pattern (panels b and e).

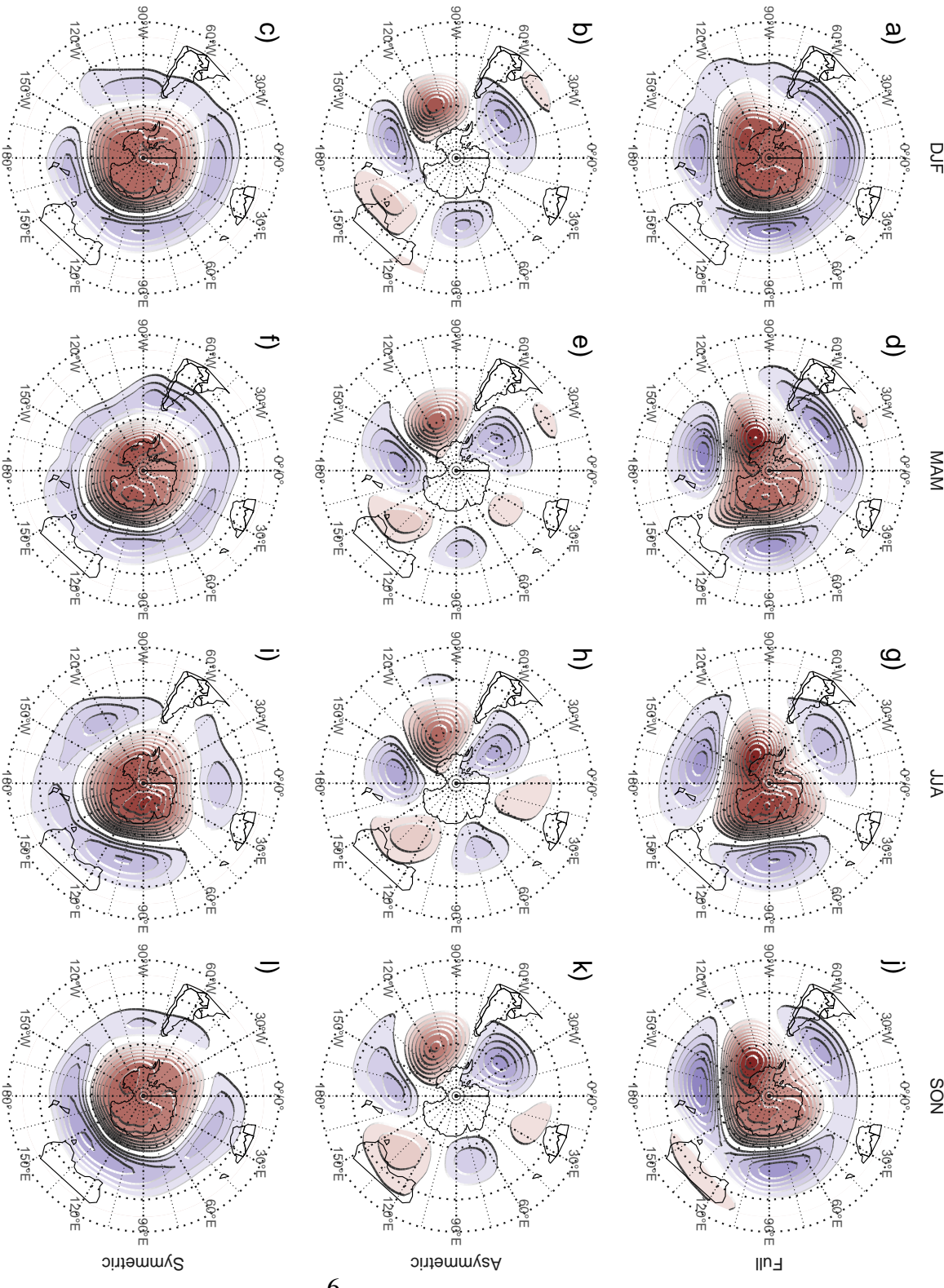


Fig. 1. Seasonal regression patterns of geopotential height at 700 hPa with the Full, Asymmetric and Symmetric SAM. The regression patterns for Asymmetric and Symmetric SAM are the result of one multiple regression using both indices, not of two simple regressions involving each index by itself.

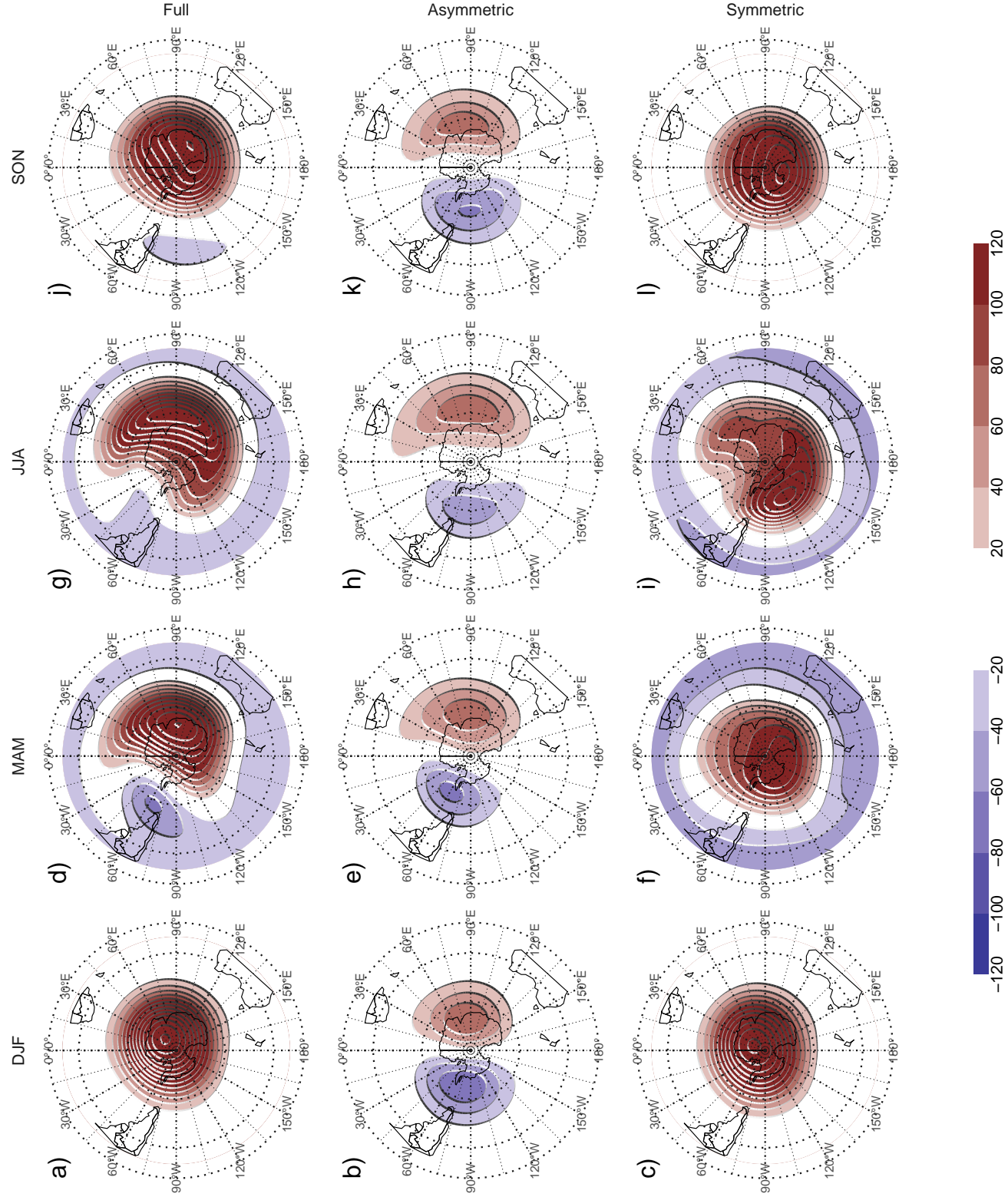


Fig. 2. Seasonal regression patterns of geopotential height at 30 hPa with the Full, Asymmetric and Symmetric SAM. The regression patterns for Asymmetric and Symmetric SAM are the result of one multiple regression using both indices, not of two simple regressions involving each index by

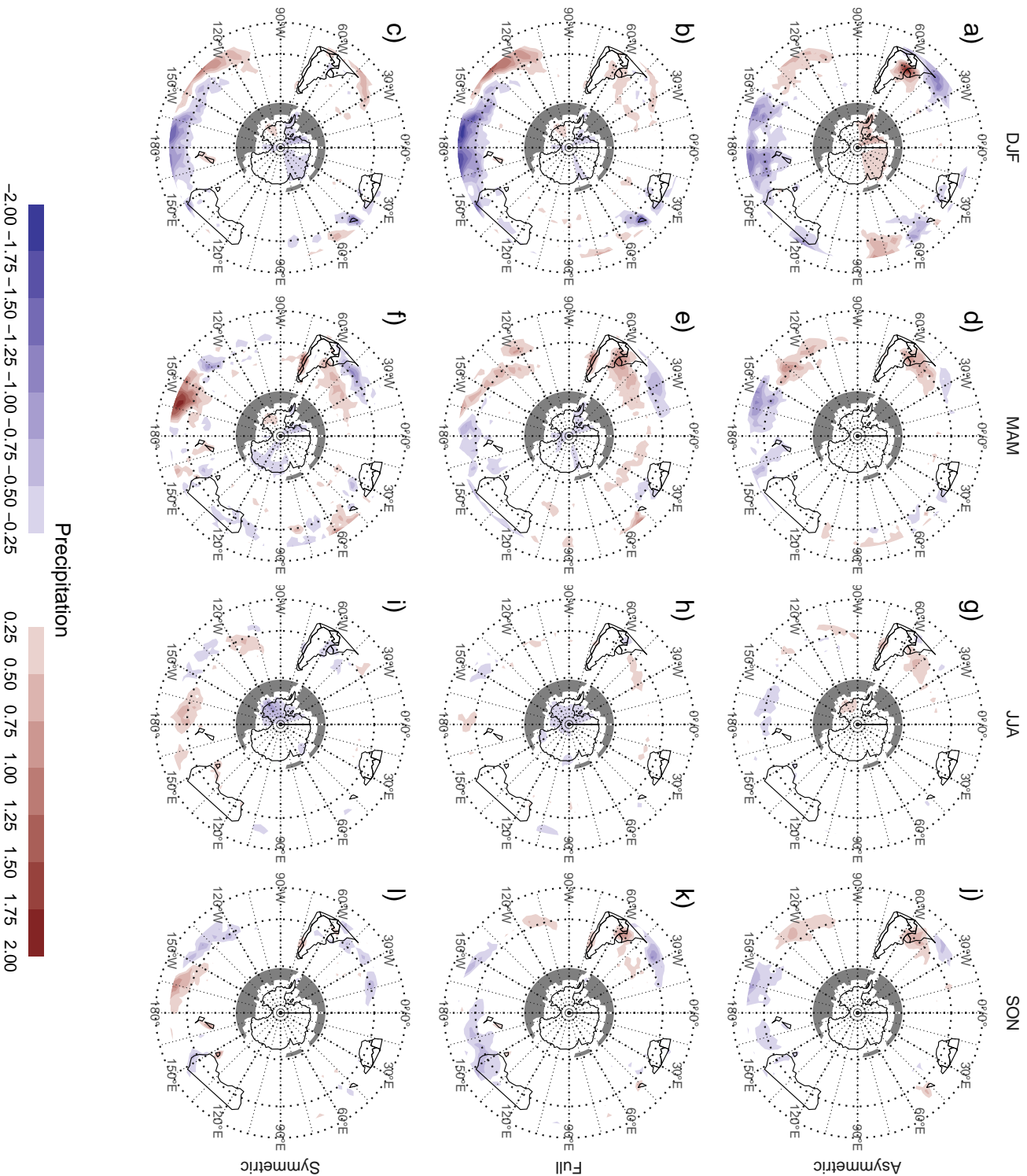


FIG. 3. Regression pattern of precipitation with Asymmetric and Symmetric SAM. P-values smaller than 0.05 (controlling for False Detection Rate)



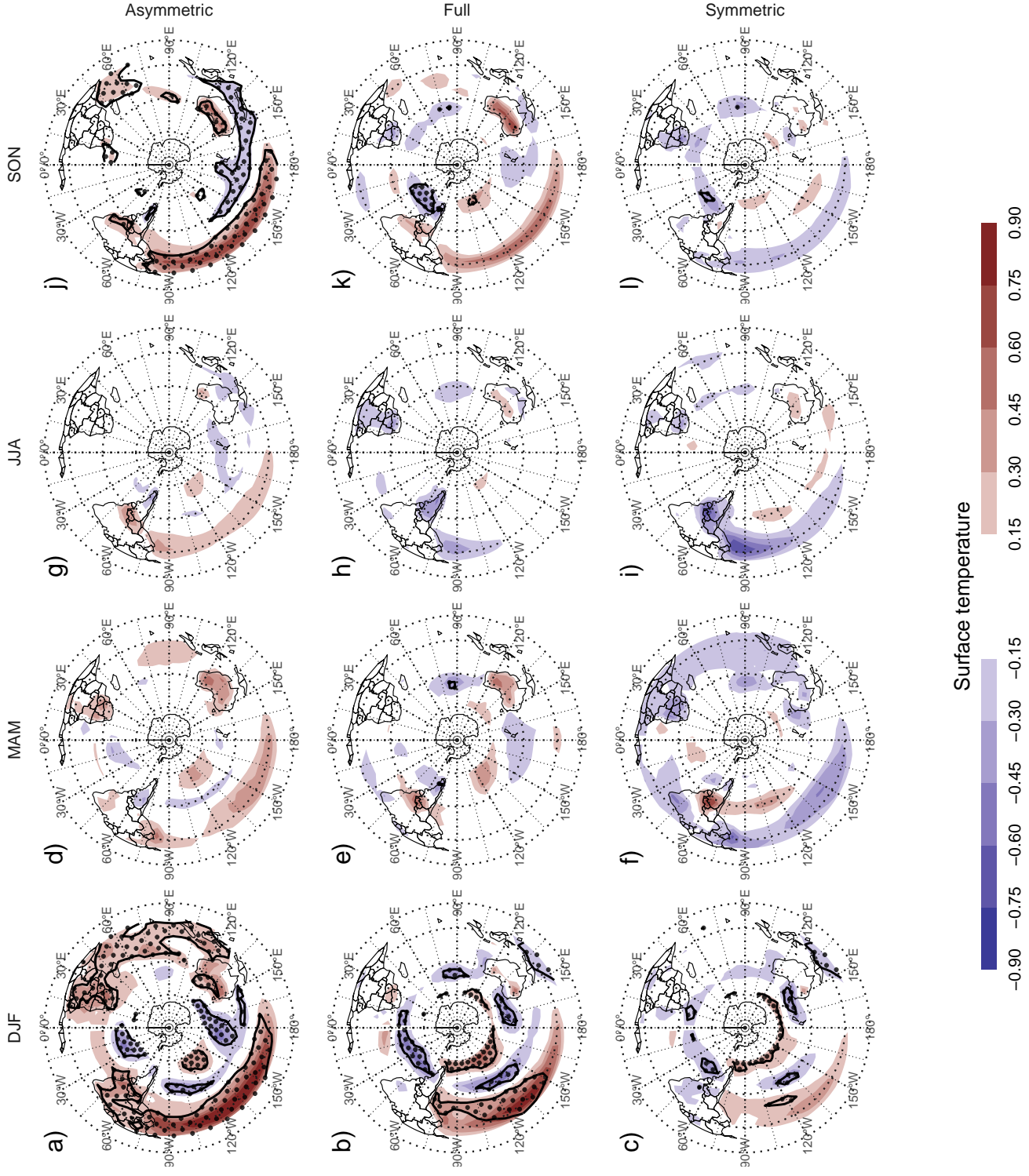


Fig. 4. Regression pattern of surface temperature with Asymmetric and Symmetric SAM. P-values smaller than 0.05 (controlling for False Detection Rate) as hatched areas.

85 *Acknowledgments.* CMAP Precipitation data provided by the NOAA/OAR/ESRL PSL, Boulder,  
86 Colorado, USA, from their Web site at <https://psl.noaa.gov/>  
87 NOAA Global Surface Temperature (NOAAGlobalTemp) data provided by the  
88 NOAA/OAR/ESRL PSL, Boulder, Colorado, USA, from their Web site at <https://psl.noaa.gov/>

## 89 **References**

90 Chung, C., and S. Nigam, 1999: Weighting of geophysical data in Principal Component  
91 Analysis. *Journal of Geophysical Research: Atmospheres*, **104 (D14)**, 16 925–16 928, doi:  
92 10.1029/1999JD900234.

93 Hersbach, H., and Coauthors, 2017: The ERA5 global reanalysis. *Quarterly Journal of the Royal*  
94 *Meteorological Society*, **n/a (n/a)**, doi:10.1002/qj.3803.

95 Osborn, T. J., and P. D. Jones, 2014: The CRUTEM4 land-surface air temperature data set:  
96 Construction, previous versions and dissemination via Google Earth. *Earth System Science*  
97 *Data*, **6 (1)**, 61–68, doi:10.5194/essd-6-61-2014.

98 Smith, T. M., R. W. Reynolds, T. C. Peterson, and J. Lawrimore, 2008: Improvements to NOAA’s  
99 Historical Merged Land–Ocean Surface Temperature Analysis (1880–2006). *J. Climate*, **21 (10)**,  
100 2283–2296, doi:10.1175/2007JCLI2100.1.

101 Vose, R. S., and Coauthors, 2012: NOAA’s Merged Land–Ocean Surface Temperature Analysis.  
102 *Bull. Amer. Meteor. Soc.*, **93 (11)**, 1677–1685, doi:10.1175/BAMS-D-11-00241.1.

103 Wilks, D. S., 2016: “The Stippling Shows Statistically Significant Grid Points”: How Research  
104 Results are Routinely Overstated and Overinterpreted, and What to Do about It. *Bull. Amer.*  
105 *Meteor. Soc.*, **97 (12)**, 2263–2273, doi:10.1175/BAMS-D-15-00267.1.

106 Xie, P., and P. A. Arkin, 1997: Global Precipitation: A 17-Year Monthly Analysis Based on  
107 Gauge Observations, Satellite Estimates, and Numerical Model Outputs. *Bull. Amer. Meteor.*  
108 *Soc.*, **78 (11)**, 2539–2558, doi:10.1175/1520-0477(1997)078<2539:GPAYMA>2.0.CO;2.

109 APPENDIX

110 **Extra figures**

111	<b>LIST OF FIGURES</b>	
112	<b>Fig. 1.</b> Seasonal regression patterns of geopotential height at 700 hPa with the Full, Asymmetric	
113	and Symmetric SAM . . . . .	6
114	<b>Fig. 2.</b> Seasonal regression patterns of geopotential height at 30 hPa with the Full, Asymmetric and	
115	Symmetric SAM . . . . .	7
116	<b>Fig. 3.</b> Regression pattern of precipitation with Asymmetric and Symmetric SAM . . . . .	8
117	<b>Fig. 4.</b> Regression pattern of surface temperature with Asymmetric and Symmetric SAM . . . . .	9
118	<b>Fig. 5.</b> Spatial patterns of the first EOF of 700 hPa geopotential height . . . . .	13
119	<b>Fig. 6.</b> Time series for the asymmetric SAM and symmetric SAM . . . . .	14
120	<b>Fig. 7.</b> Correlation between the Symmetric and Asymmetric SAM at each level . . . . .	15
121	<b>Fig. 8.</b> Cross correlation between levels of the Full, Asymmetric and Symmetric SAM . . . . .	16
122	<b>Fig. 9.</b> Regression patterns of geopotential height at 30, 300 and 700 hPa with the Full, Asymmetric	
123	and Symmetric SAM . . . . .	17
124	<b>Fig. 10.</b> Asymmetric coefficient of the multiple regression of mean monthly geopotential height	
125	anomalies between 65 and 40 South . . . . .	18
126	<b>Fig. 11.</b> Planetary wave amplitude for the regression patterns at 700 hPa . . . . .	19
127	<b>Fig. 12.</b> Planetary wave amplitude for the regression patterns at 30 hPa . . . . .	20
128	<b>Fig. A1.</b> Lag-correlation between Symmetric and Asymmetric SAM at each level. . . . .	21
129	<b>Fig. 13.</b> Cross-correlation functions for each index and two different base levels . . . . .	22
130	<b>Fig. A2.</b> Fourier spectrum of each timeseries. The shading indicates the 95% area derived by fitting	
131	an AR process to each series and bootstrapping 5000 simulated samples. . . . .	23
132	<b>Fig. A3.</b> Autocorrelation functions of each timeseries . . . . .	24
133	<b>Fig. A4.</b> Trends for each index at each level. Shading indicates the 95% confidence interval. . . . .	25
134	<b>Fig. A5.</b> Regression pattern of precipitation with Asymmetric and Symmetric SAM. P-values smaller	
135	than 0.05 (controlling for False Detection Rate) as hatched areas. . . . .	26
136	<b>Fig. A6.</b> Regressions maps resulting from performing one multiple regression (a. and b.) and from	
137	performing two simple regressions (c. and d.) . . . . .	27

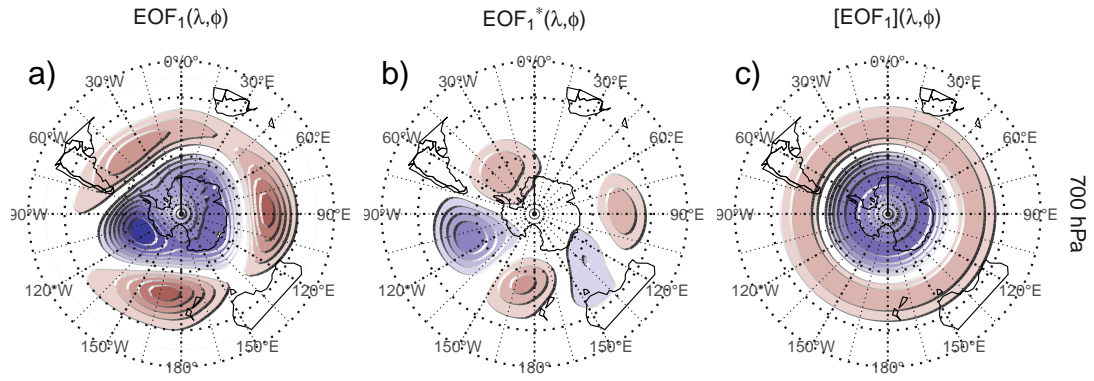


FIG. 5. Spatial patterns of the first EOF of 700 hPa geopotential height. Full field (left), zonally asymmetric  
 component (middle) and zonally symmetric component (right). Arbitrary units.

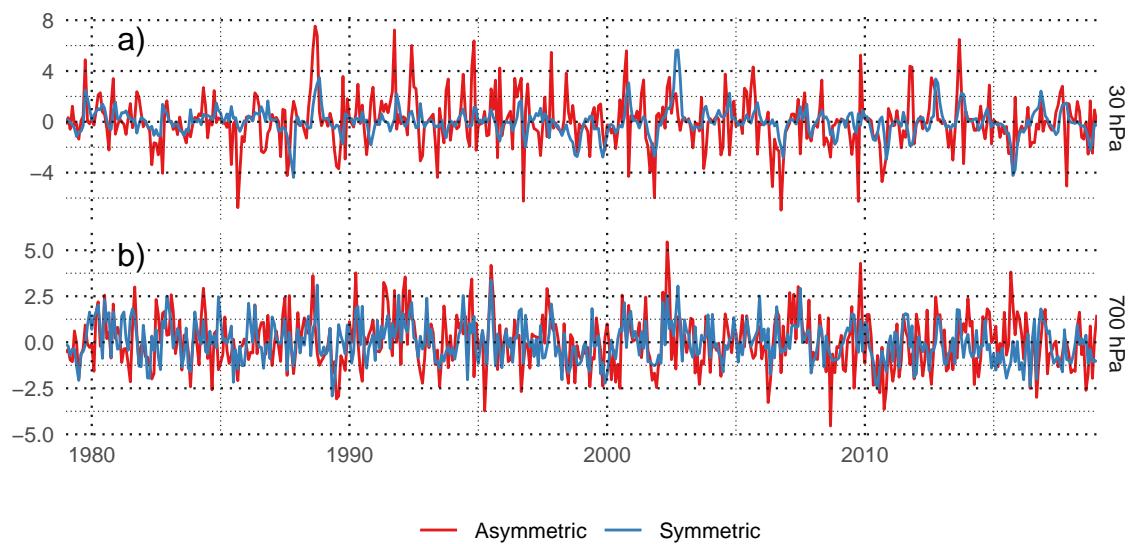


FIG. 6. Time series for the asymmetric SAM and symmetric SAM.

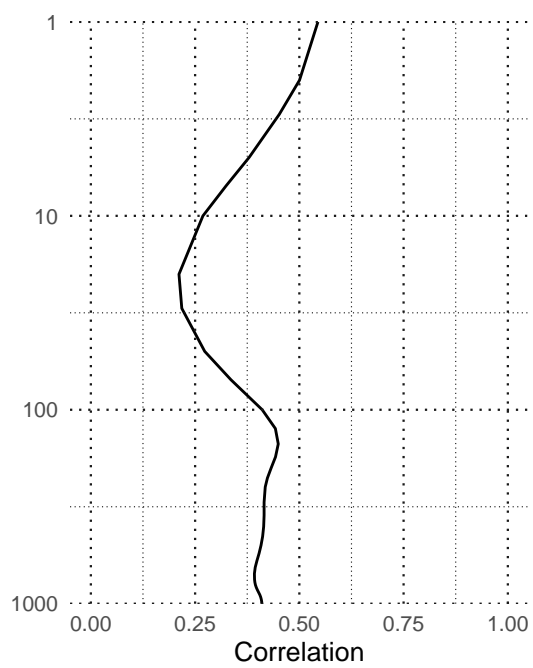


FIG. 7. Correlation between the Symmetric and Asymmetric SAM at each level.

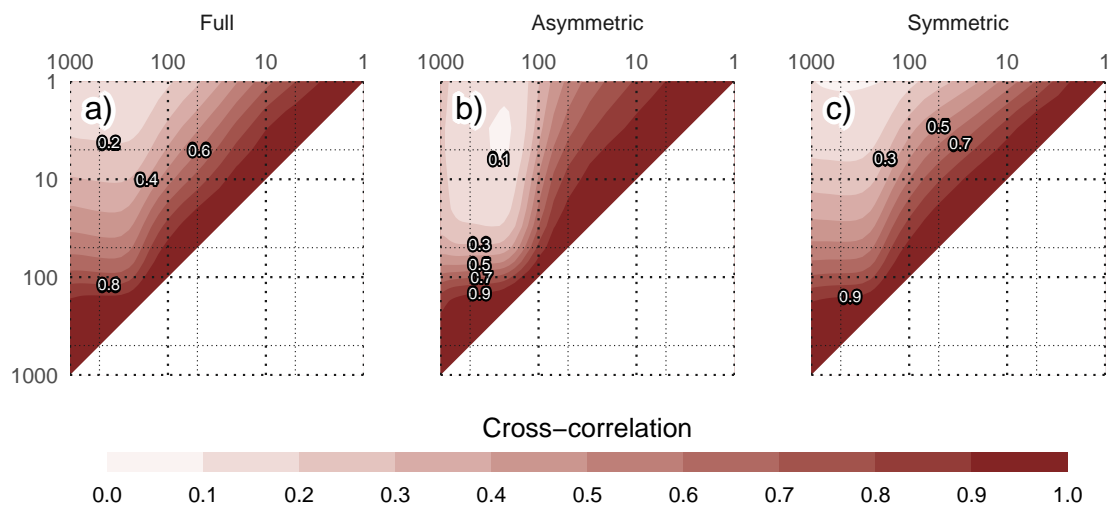


FIG. 8. Cross correlation between levels of the Full, Asymmetric and Symmetric SAM.



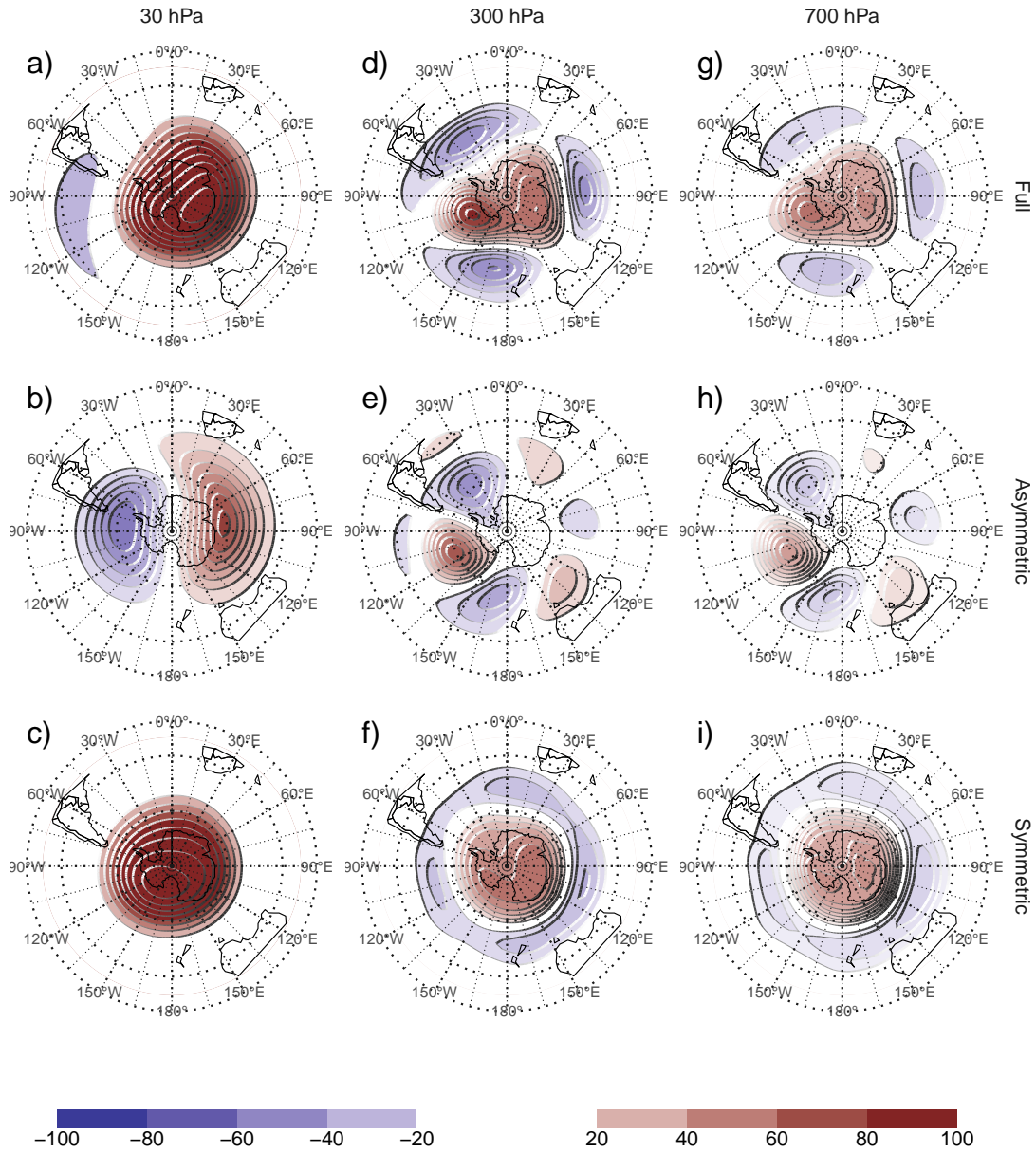


FIG. 9. Regression patterns of geopotential height at 30, 300 and 700 hPa with the Full, Asymmetric and Symmetric SAM. The regression patterns for Asymmetric and Symmetric SAM are the result of one multiple regression using both indices, not of two simple regressions involving each index by itself.

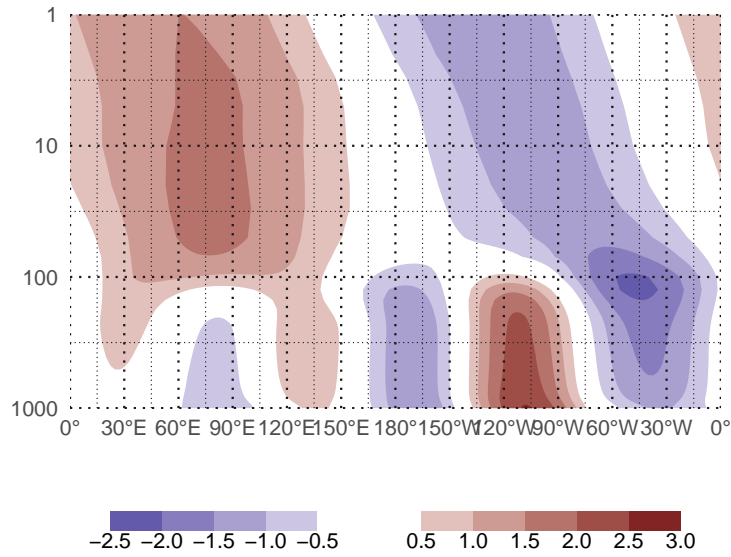


FIG. 10. Asymmetric coefficient of the multiple regression of mean monthly geopotential height anomalies between 65 and 40 South. Values are standardised by the standard deviation at each level. (this caption needs some love)

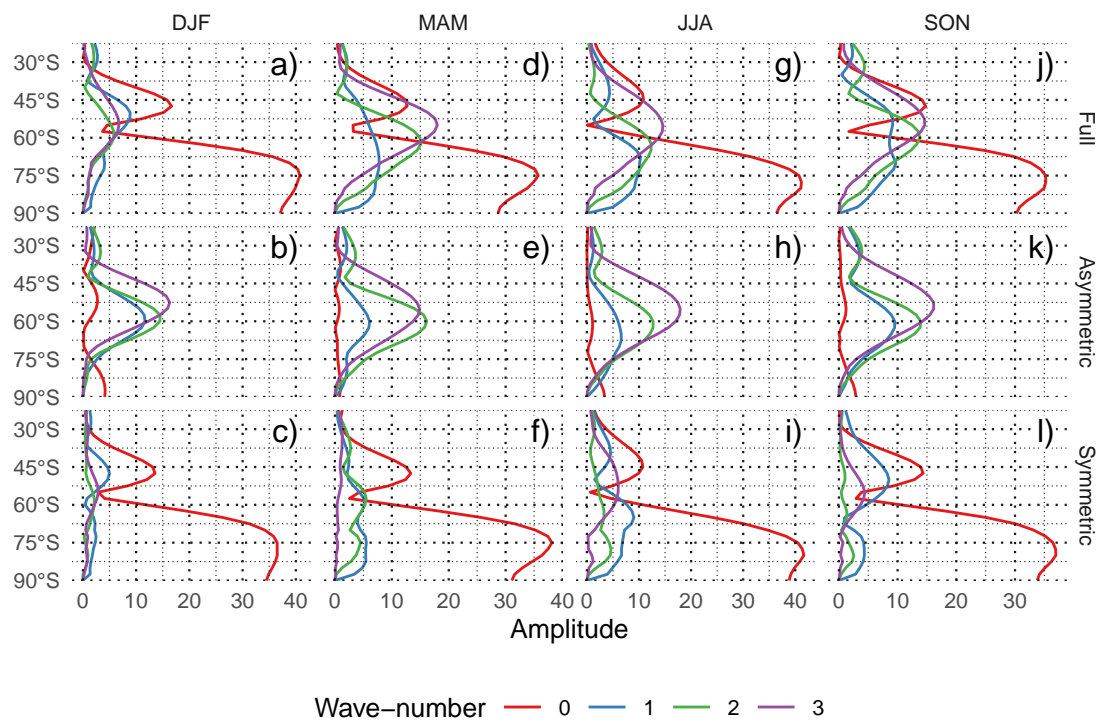


FIG. 11. Planetary wave amplitude for the regression patterns at 700 hPa.

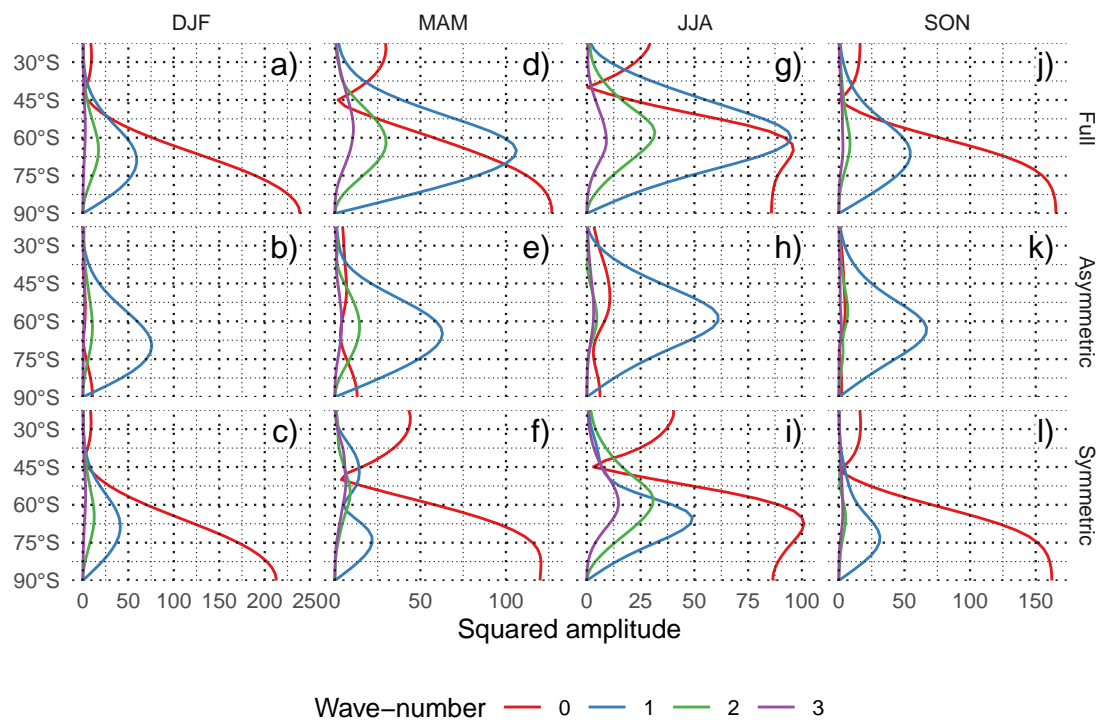


FIG. 12. Planetary wave amplitude for the regression patterns at 30 hPa.

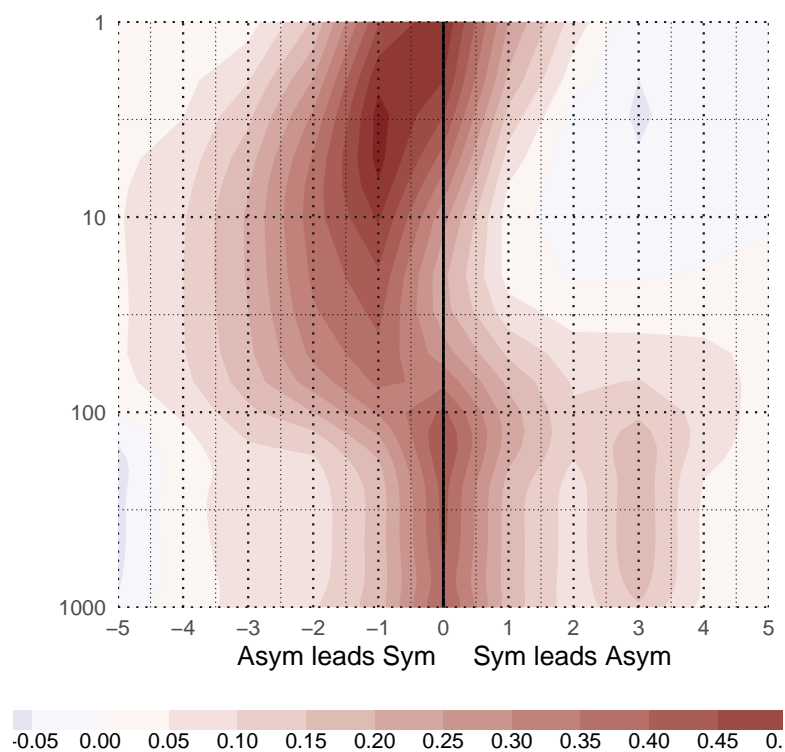


Fig. A1. Lag-correlation between Symmetric and Asymmetric SAM at each level.

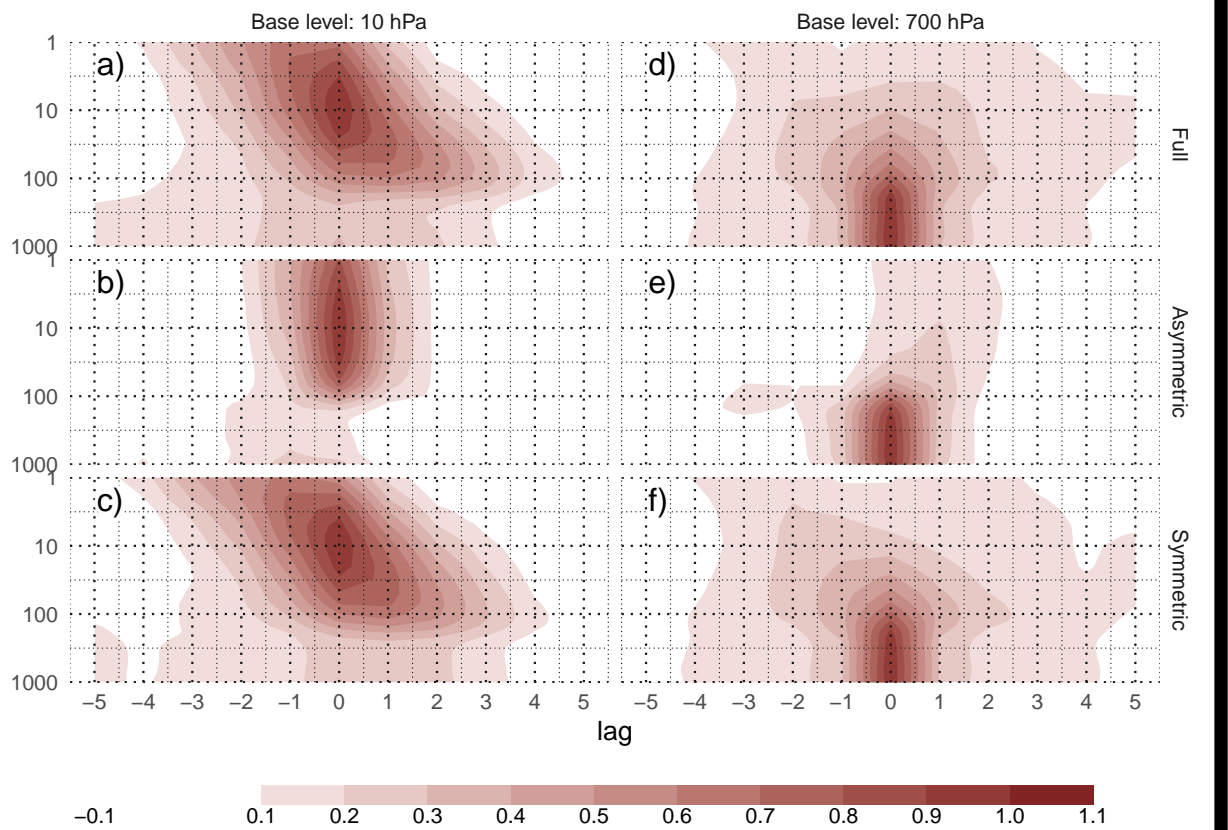


FIG. 13. Cross-correlation functions for each index and two different base levels.

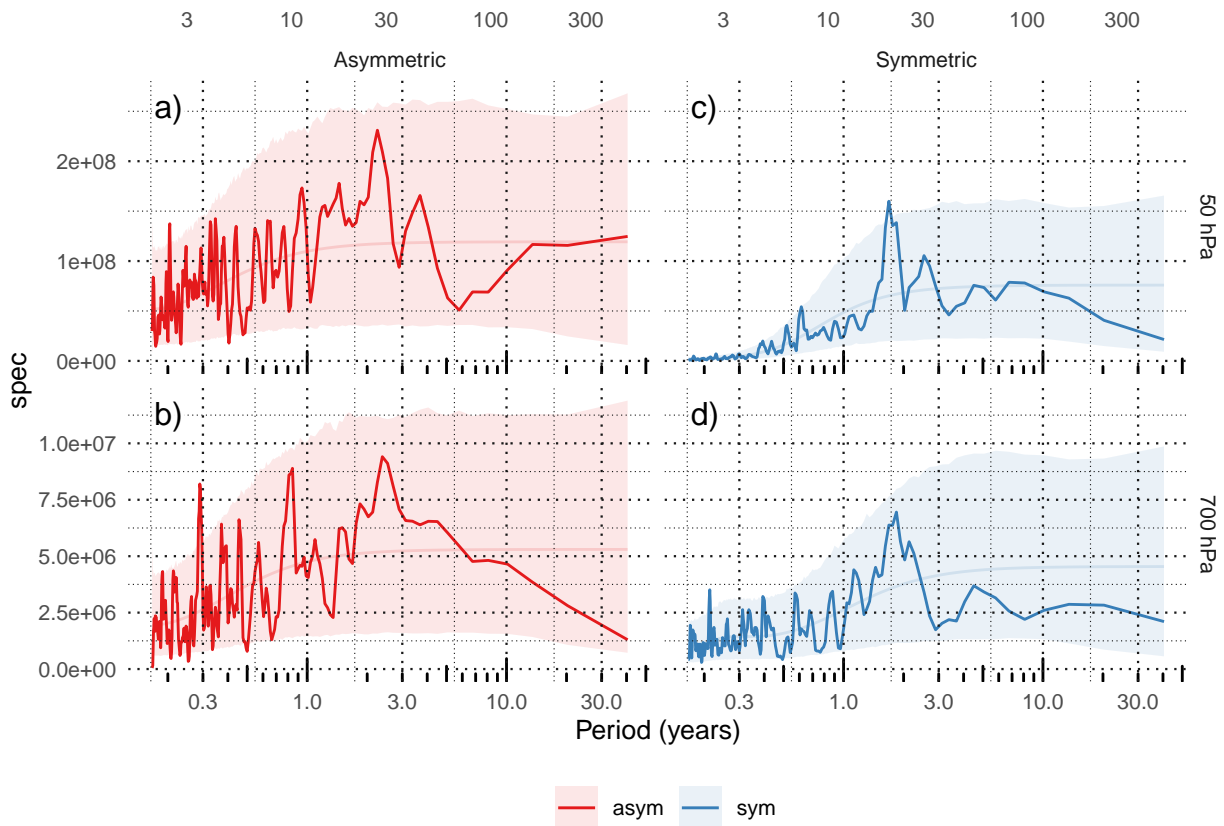


Fig. A2. Fourier spectrum of each timeseries. The shading indicates the 95% area derived by fitting an AR process to each series and bootstrapping 5000 simulated samples.

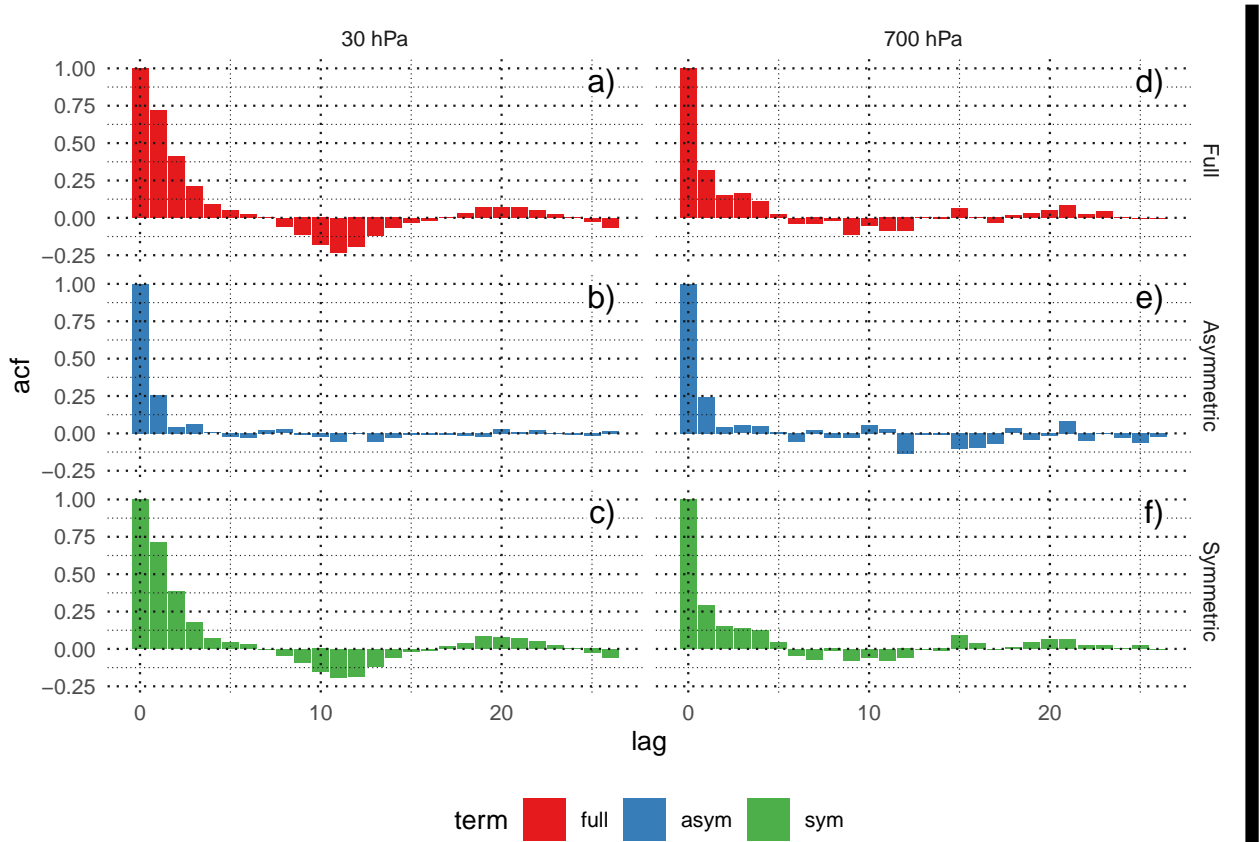


Fig. A3. Autocorrelation functions of each timeseries



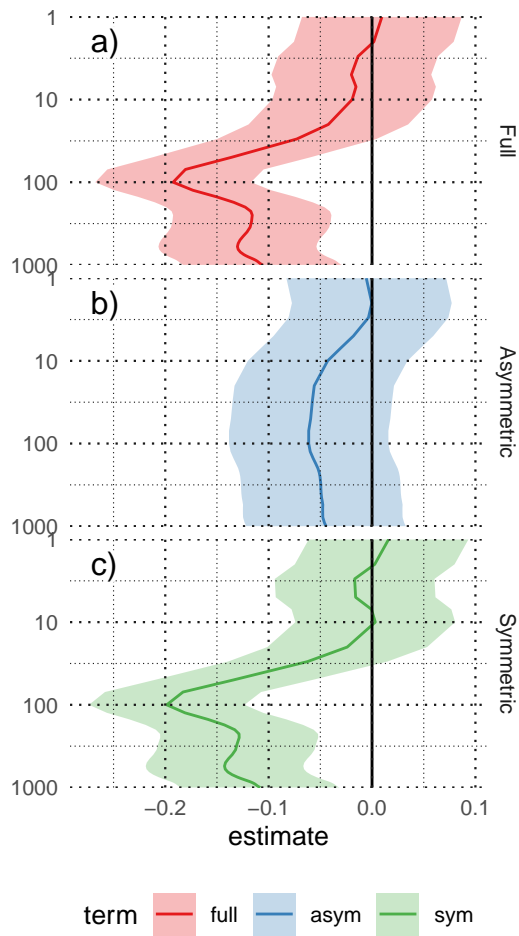


Fig. A4. Trends for each index at each level. Shading indicates the 95% confidence interval.

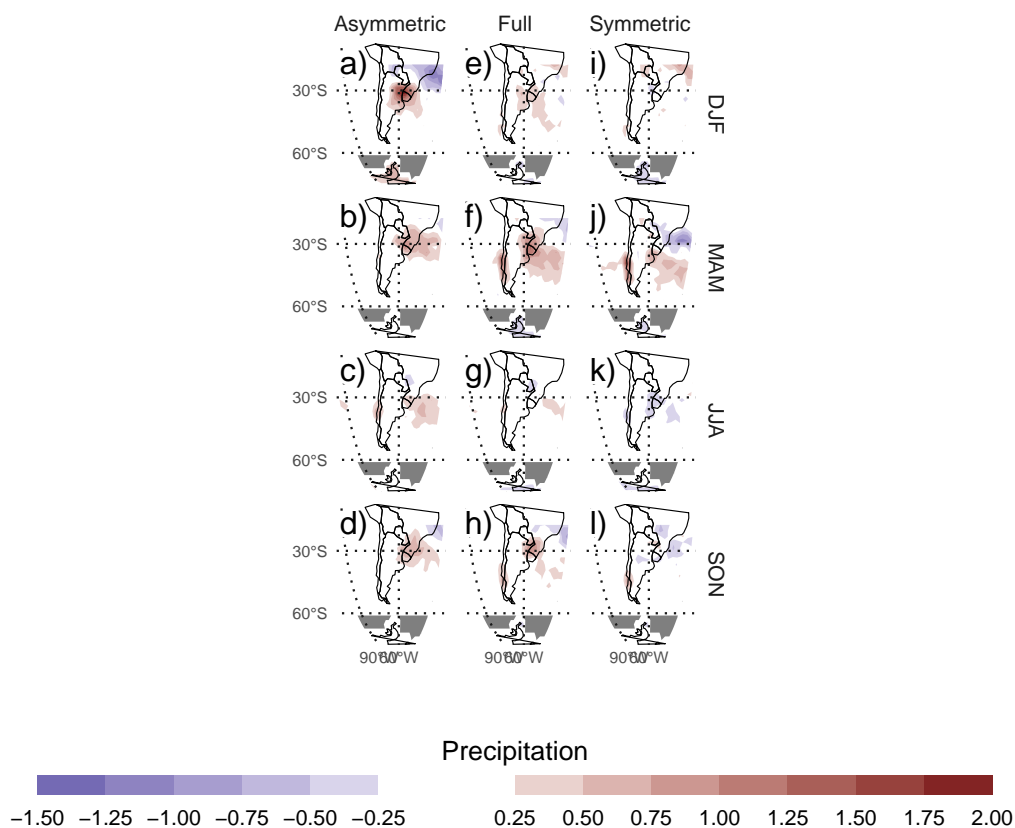
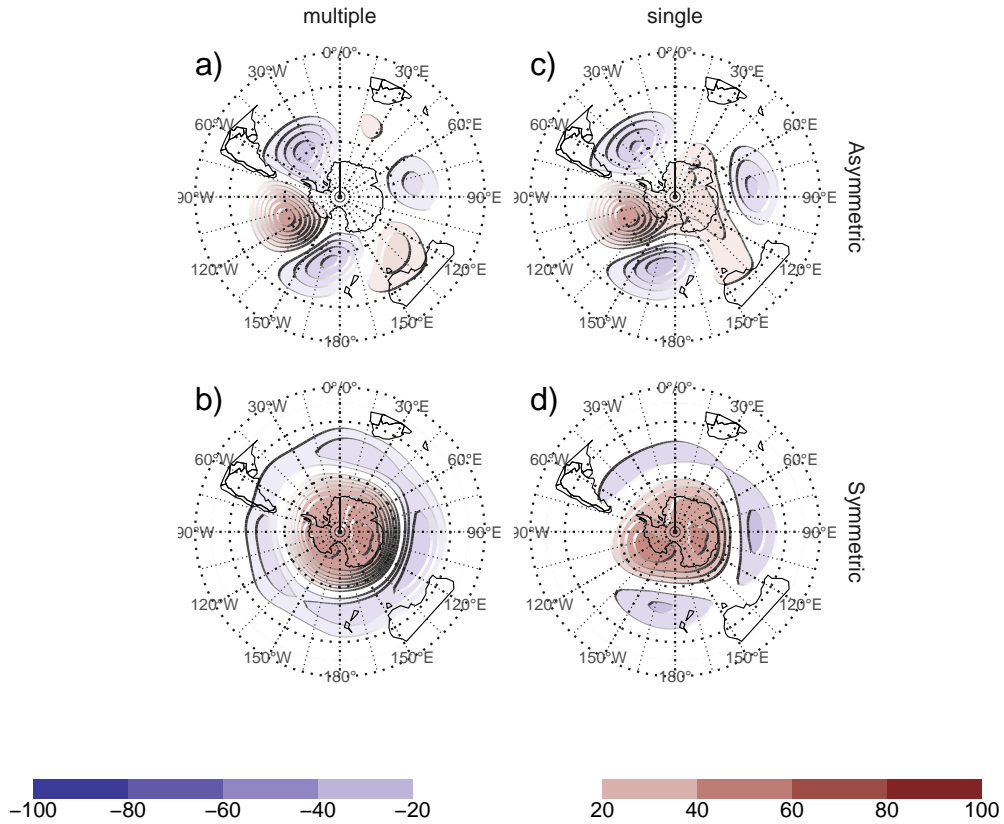


Fig. A5. Regression pattern of precipitation with Asymmetric and Symmetric SAM. P-values smaller than 0.05 (controlling for False Detection Rate) as hatched areas.



150 Fig. A6. Regressions maps resulting from performing one multiple regression (a. and b.) and from performing  
 151 two simple regressions (c. and d.)